CloudSat Project

A NASA Earth System Science Pathfinder Mission

Level 2C CloudSat-CALIPSO Combined Ice Cloud Property Retrieval Product Process Description Document

Version: P1_R04

Document Version: 0.

Date: 04 November 2015

Questions concerning the document and proposed changes shall be addressed to

Gerald Mace
mace@met.utah.edu
(801) 585-9489

or

Min Deng
mdeng2@uwyo.edu
(307) 766-6334

Table of Contents

1 Introduction

The Cloudsat and CALIPSO Ice Cloud Property Product (2C-ICE) contains retrieved estimates of ice cloud water content (IWC), effective radius (r_e) and extinction coefficient for identified ice clouds measured by Cloud profiling Radar (CPR) on CloudSat or the CALIPSO Cloud-Aerosol Lidar with Orthogonal Polarization (CALIOP; hereafter referred as the Lidar). This 2C-ICE cloud product uses combined inputs of measured radar reflectivity factor from the CloudSat 2B-GEOGPROF product and measured attenuated backscattering coefficients at 532 nm from CALISPO lidar to constrain the ice cloud retrieval more tightly than the radar-only product and to generate more accurate results.

Because the CPR and CALIOP probe the atmosphere using such vastly separated components of the electromagnetic spectrum, the information provided by the two instruments contains information about very different parts of the particle distribution in any given sample volume. The radar reflectivity contains information from the largest set of particles while the backscattered lidar energy responds much more to the smaller particles that contribute to the physical cross sectional area within the volume. However, the macroscopic characteristics of the observations such as vertical resolution and spatial resolution are quite different from one another. Collocating CALIPSO lidar observed attenuated backscattering coefficients to CloudSat spatial resolution is first performed to combine the two data streams.

The characteristics of the instruments convolved on the physical properties of clouds in the upper troposphere require us to consider that three distinct regions can generally exist in any ice cloud layer as shown in figure 1. A region of tenuous clouds will exist above the region where the radar and lidar both sense the presence of cloud. There will often also be a region below which the lidar signal has fully attenuated but the radar continues to return data. The radar signal will be not generally fully attenuated in thick ice clouds; however, some attenuation may occur in heavy thunderstorm anvils. An algorithm must allow for the occurrence of any or all of these distinct regions in its formulation and recognize that the presence or absence of signal as well as the structure of the vertical profile provides specific information about the layer. For instance, in lidar only region, while we don't know the radar reflectivity, we do know that it is less than the minimum detectable signal of the CPR. Also in radar only, while we don't know the attenuated backscatter, we do know that enough optical path exists above to fully attenuate the lidar signal and the structure of the radar return does provide empirical information about the extinction (Matrosov et al., 2003).

This document describes the 2C-ICE algorithm that will be implemented operationally to combine the CPR and Lidar data to meet the goals described above. For each profile, the algorithm will:

- Exam the cloud mask in 2B-GEOPROF-LIDAR and cloud type and phase in 2B-CLDCLASS-Lidar to identify the ice cloud; Identify the distinct instrument observation zones based on radar mask from 2B-GEOPROF and lidar mask from LIDAR-AUX;

- Assign a priori values of ice cloud water content and effective radius based on lidar estimated extinction coefficient, climatology, temperature and other criteria;

- Use the a priori values and radar measurements from 2B-GEOPROF and lidar measurement from LIDAR-AUX to retrieve ice cloud water content, effective radius, extinction for each cloudy bin;

- Calculate uncertainties for each of these estimates, and estimate the retrieval status according to convergence analysis.

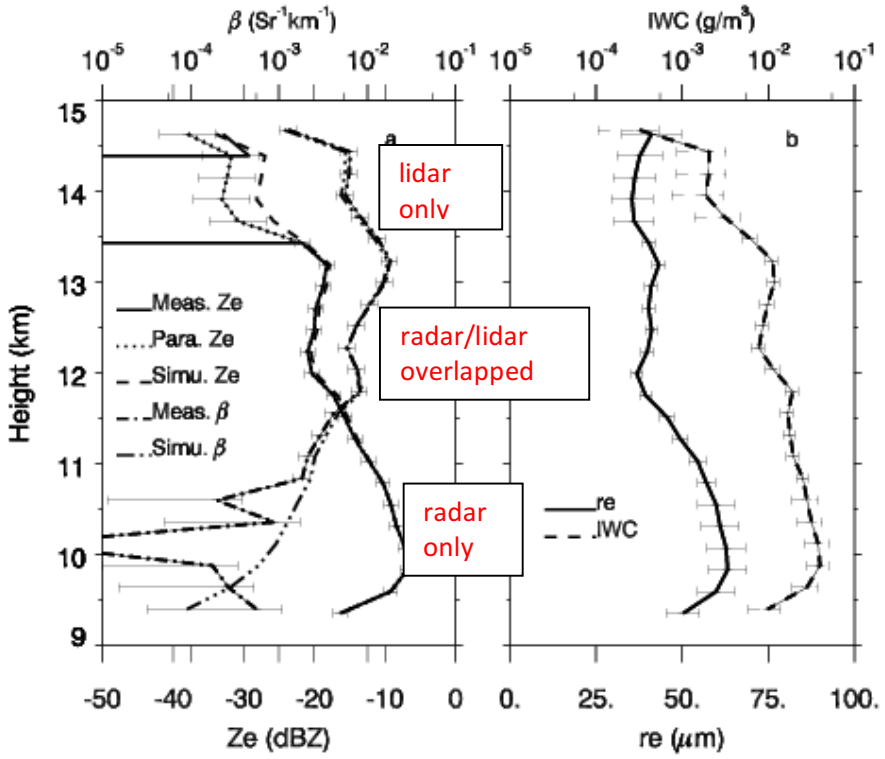

Figure 1. The CPR reflectivity (Ze) and CALIPSO lidar attenuated backscattering (β) profiles (a) and retrieved r_e and IWC profiles (b). The horizontal bars are the measurement error and retrieval error in (a) and (b), respectively. Also plotted in (a) are parameterized CPR reflectivity (dot), simulated CPR reflectivity (dash) and attenuated backscattering (dash-dot-dot).

2 Algorithm Theoretical Basis

The ice cloud retrieval algorithm description in the section is a condensed version of the method described in Deng et al (2010), together with updated ice cloud identification method, convergence analysis and validation studies. The algorithm flowchart is shown in figure 2. We will describe the key parts of the algorithm in this figure in the following.

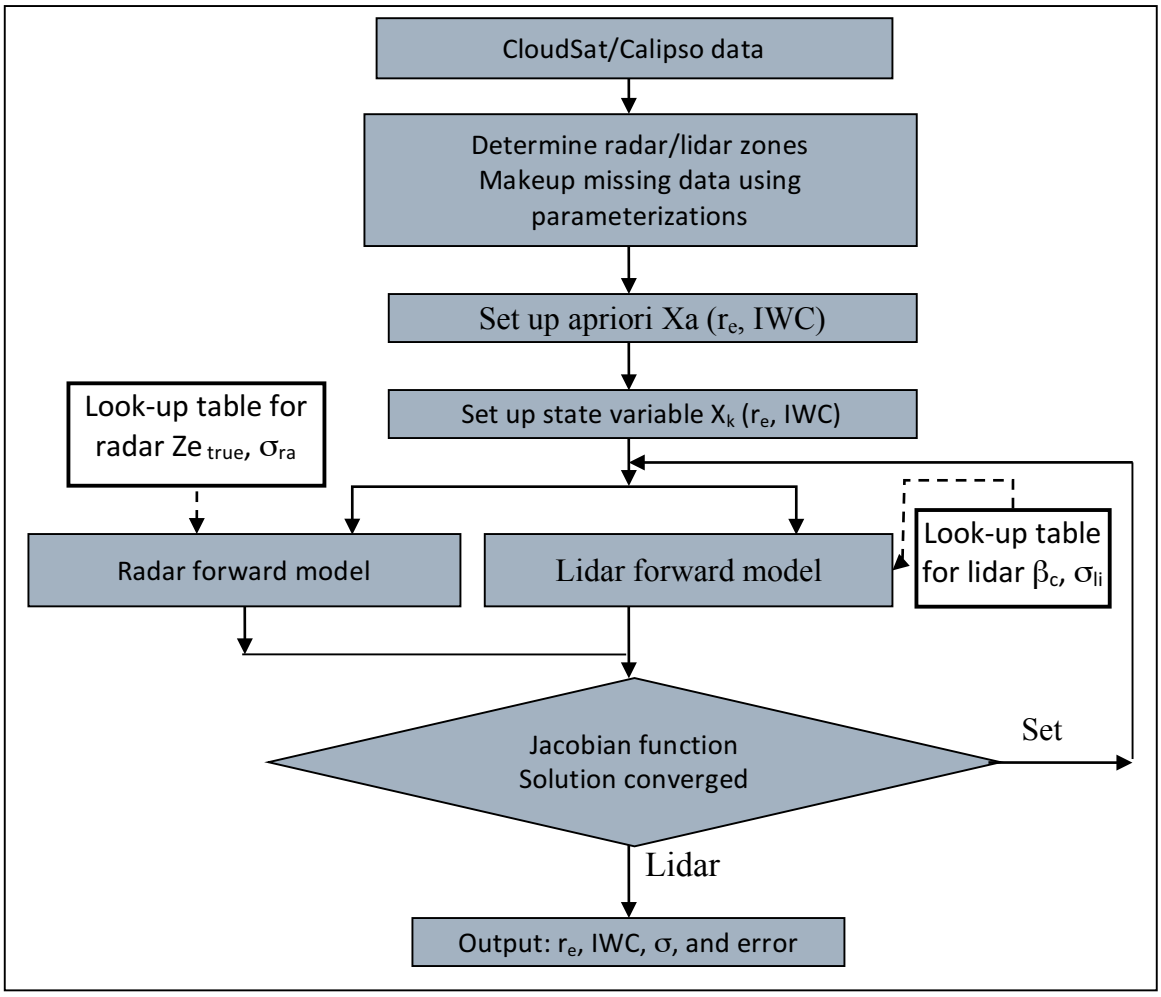

Figure 2. The flowchart of 2C-ICE product to retrieve ice cloud re and IWC from combined CloudSat CPR and CALIPSO lidar measurements.

2.1 Formulations of Variation Estimation

The algorithm is built upon an optimal estimation framework [Rogers, 2000]. In this framework we consider a state vector, *x (*i.e. r_e *and IWC)*, that describes the properties of the vertical profile of ice cloud microphysics that result in a set of lidar attenuated backscattering coefficients (β') and radar reflectivity factor (Z_e) measurements expressed as vector *y*.

$$x = \begin{bmatrix} r_{e1} \\ r_{e2} \\ r_{e3} \\ \vdots \\ r_{en} \\ IWC_1 \\ IWC_2 \\ IWC_3 \\ \vdots \\ IWC_n \end{bmatrix} \qquad y = \begin{bmatrix} \ln \beta'_1 \\ \ln \beta'_2 \\ \ln \beta'_3 \\ \vdots \\ \ln \beta'_n \\ \ln Z_{e1} \\ \ln Z_{e2} \\ \ln Z_{e3} \\ \vdots \\ \ln Z_{en} \end{bmatrix} \tag{1}$$

where n is the CloudSat range bins of a cloudy layer. The relationships linking the atmospheric state and the measurements are the forward model i.e.

$$y = F(x, b) + \varepsilon \tag{2}$$

where *b* are parameters used in the forward model *F*. The inverse problem can be approximated using Bayes theorem where we maximize the a posteriori likelihood of *x* given *y*. The solution is typically found by iteration by initializing a state vector *x* with an *a priori* (x_a) estimation from extensive in situ measurements or empirical relations or algorithms in the literature. Using Gauss-Newton iteration, an expression for the state vector can be expressed:

$$x_{i+1} = x_i + (S_a^{-1} + K_i^T S_\varepsilon^{-1} K_i)^{-1} [K_i^T S_\varepsilon^{-1} (y - F(x_i)) - S_a^{-1} (x_i - x_a)] \tag{3}$$

where *K* is the Jacobian matrix containing the derivatives of each observation with respect to each state vector. S_a and S_ε are the error covariance matrices chosen to limit the amount of bias of a priori and measurement from the true state vector and ideal measurements, respectively. The error covariance matrices are assumed diagonal in the present implementation.

Given the *state vector*, a *forward model* can be applied to predict what measurements the instruments would observe. By comparing these predictions with the measurements actually observed, and by making use of additional information provided by the forward model calculation (namely derivatives of measurement with respect to the state vector, i.e. the *Jacobian matrix*), the retrieval algorithm iteratively computes a better estimate of the state vector, i.e. one for which the predicted measurements will be closer to those observed. The retrieval algorithm adjusts the state vector until appropriate *convergence* has been achieved.

2.2 Physics of Forward Models

2.2.1 Lidar Forward Model

The lidar equation for attenuated backscattering coefficient, β', can be expressed generally as:

$$\beta'(R) = [\beta_c(R) + \beta_m(R)]\exp\{-2\int_0^R \eta(r)\sigma_{li}(r)dr\} \tag{4}$$

where R is the range, $\beta_c(R)$, $\beta_m(R)$ and $\sigma_{li}(R)$ are the particle and molecular lidar backscattering coefficients and total extinction coefficient at the lidar wavelength, respectively. η is a multiple scattering correction factor (Platt 1998). The molecular lidar backscattering coefficient can be calculated according to the thermodynamic state of the atmosphere provided by the ECMWF-AUX dataset.

The CALIOP lidar has a large footprint compared with ground-based or airborne lidars, which allows a greater contribution of the multiple-scattered light to the total return signal. The multiple scattering effects can influence the apparent extinction or transmittance of the medium. Therefore, multiple scattering effects must be accounted for in the algorithm to retrieve accurate cloud extinction coefficient and optical depth as well as IWC and r_e. In principle, the multiple scattering contributions to the lidar signal [Battaglia et al., 2007; Hogan, 2006; Eloranta, 1998] usually is derived from either a Monte Carlo method or is computed from analytical approximation. However, we adopt a single η as a constant (0.6), it makes the lidar forward model and hence the entire algorithm faster, which is necessary for an operational algorithm that is to be applied to a large amount of global data. .

For a layer with finite thickness, the attenuation term is modified following Okamoto (2003) as:

$$\beta'(R_i) = [\beta_c(R_i) + \beta_m(R_i)]\exp\{-2\int_0^{R_{i-1/2}} \eta\sigma_{li}(r)dr\}\{\frac{\exp[-2\sigma_{li}(R_i)\Delta R]-1}{-2\sigma_{li}(R_i)\Delta R}\} \tag{5}$$

where R_i denotes the altitude of the center of the layer i. $R_{i-1/2}$ is the top boundary of the cloud layer i. ΔR is the vertical resolution. The first term on the right is the particle and molecular backscatter before attenuation. The second term accounts for two way attenuation due to gasses and particles and accounted for multiple scattering effect with an η. The third term accounts for the attenuation and multiple scattering within the range resolution volume – a potential issue for the coarse vertical resolutions of Cloudsat and CALIPSO. The particle backscatter and extinction coefficients are calculated for certain PSD and certain particle habits as a part of the look-up-table discussed in section 2.3

2.2.2 Radar Forward Model

For the CloudSat CPR signal, we apply a similar analysis as for the lidar following Okamoto 2003:

$$Z_e'(R_i) = Ze_{tru}(R_i)\exp\{-2\int_0^{R_{i-1/2}} \sigma_{ra}(r)dr\}\{\frac{\exp[-2\sigma_{ra}(R_i)\Delta R]-1}{-2\sigma_{ra}(R_i)\Delta R}\} \quad (6)$$

Z_e' and Ze_{true} are the observed Z_e and true Z_e (the radar reflectivity that would be observed without particle attenuation), respectively. σ_{ra} is the extinction coefficient at radar wavelength. Ze_{true} and σ_{ra} are calculated for certain PSD and certain particle habits as a part of the look-up-table discussed in section 2.3.

The last part of the forward model includes the calculation of the Jacobian that contains the derivative of measurements respective to each element of the state vector and parameters used in the forward model such as the multiple scattering factor. Since attenuation is included in both the lidar and radar forward model and the attenuation is only relative to the path before that range gate measured, causing the lower triangular terms in the Jacobian matrices to be zero.

Equations 5 and 6 represent the forward model *F(x)*. Because the solution algorithm assumes a nonlinear relationship between y and x, we express the forward model equations 5 and 6 in terms of the natural logarithm of Z_e and β'. The use of logarithms in y also results in faster convergence to the correct solution as indicated by Delanoe and Hogan [2008].

2.3 Cloud Microphysical Model and Look Up Table

The look-up table contains the bulk microphysical relations between IWC, r_e, β_c, σ_{li}, σ_{ra} and Ze_{true} of ice particles in the CPR sample volume. It depends on a microphysical model, which describes the functional shape of the PSD, and relationships between the particle mass, cross sectional area and particle size. The backscattering and extinction coefficients at lidar and radar wavelengths are related to the particle size distribution function as the following:

$$\beta_c(R) = \frac{1}{4\pi}\int_{D\min}^{Dmas} N(D)C_{bk}(D,R)dD \quad (7)$$

$$\sigma_{li}(R) = \int_{D\min}^{Dmas} N(D)C_{ext,li}(D,R)dD \quad (8)$$

$$\sigma_{ra}(R) = \int_{D\min}^{Dmas} N(D)C_{ext,ra}(D,R)dD \quad (9)$$

$$Ze_{true}(R) = \frac{\lambda^4}{\pi^5 |K|^2}\int_{D\min}^{Dmas} N(D)C_{bk}(D,R)dD \quad (10)$$

where $C_{bk,li}$, $C_{bk,ra}$, $C_{ext,li}$, $C_{ext,ra}$ are the backscattering and extinction cross sections at the lidar and radar wavelengths, respectively. K is estimated from the complex refractive index of water. $N(D)$ is the PSD, here we assume a modified Gamma PSD:

$$N(D) = N_g e^{\alpha} (\frac{D}{D_g})^{\alpha} \exp\left[-\alpha \frac{D}{D_g} \right] \tag{11}$$

where D is the particle maximum length, N_g is a proportionality constant, D_g is the size where the function $N(D)$ maximizes, and α indicates the breadth of the spectrum. Instead of retrieving particle size distribution parameters, we retrieve r_e and IWC. r_e is defined as:

$$r_e = \frac{3}{4} \frac{Volume}{Area} = \frac{3}{4} \frac{\frac{1}{\rho_{ice}} \int_{D\min}^{D\max} a_m D^{b_m} N(D) dD}{\int_{D\min}^{D\max} a_a D^{b_a} N(D) dD} \tag{12}$$

where a_m and b_m are the parameters in a mass and size power law relation, a_a and b_a are the parameters in an area and size power law relation [Brown and Francis, 1995; MacFarquhar et al., 1999; Baum et al 2005, Deng and Mace, 2006], ρ_{ice} is the density of solid ice. The dimensional power law relation parameters are different for different crystal habits and shapes, and they are from directed calculation assuming certain particle habits or shape [Yang et al 2000]. To test the effects of particle habit assumptions on retrieval accuracy, we build up several look-up tables (Figure 3) with different particle habits (sphere, hexagonal plate, column, bullet rosette or aggregate), which are assumed to be oriented randomly. The extinction properties of nonspherical ice crystals at 532nm are computed by accurate light scattering calculations and parameterized by Yang et al. [2000]. The backscattering properties at 532 nm are calculated from extinction coefficients assuming a constant lidar ratio 30. For 94 GHz, the backscattering properties were reported by Yang et al. [2000]. We can develop one dimensional look-up tables normalized by IWC to relate r_e to β_c, σ_{li}, σ_{ra} and Ze_{true}.

2.4 A Priori Data and Covariance

A priori estimation of r_e and IWC and the associated error covariance matrix represent prior knowledge that can be incorporated to improve our estimation and the deviation of the element of the true state from the a priori. The prior knowledge can come from empirical relations derived from extensive in situ measurements, such as IWC and Z_e relations [Liu and Illingworth, 2000] or the relation between normalized number concentration and temperature [Delanoe and Hogan, 2008], or from other validated algorithm estimations in the literature. In the current algorithm, we use both empirical relations and retrievals from published algorithms for prior knowledge. Because CloudSat and CALIPSO measurements contain enough information to constrain r_e and IWC retrievals, the retrieval results are less dependent on the a priori. Thus, the a priori covariance matrix S_a, the diagonal values are simply set to as twice as the a priori estimation, which make the a priori information weighs less than the measurements. Our goal to set up a priori to speed up the retrieval (converge in less iteration).

As an example, for the thin cirrus clouds the lidar can penetrate the entire layer and the layer transmittance can be estimated from the lidar return below the layer base. This transmittance can

then be used as a constraint in performing the extinction coefficient retrieval using Fernald [1972] backward iteration. With the parameterized radar reflectivity and extinction coefficient from Fernald iteration, r_e and IWC can then be estimated using the lidar/radar algorithm developed by Wang and Sassen [2002] and be used as a priori. For thick cirrus layers, the lidar signal becomes attenuated below the radar/lidar overlapped region. According to Austin et al. [2009], the ice cloud microphysical parameters such as r_e and IWC can be estimated using the CPR reflectivity and temperature as a priori. However, for the radar/lidar overlapped region, r_e and IWC retrieved by combining extinction and Z_e with the algorithm of Wang and Sassen [2002] can be used as better a priori.

The covariance of the state vector, x, can be calculated from the covariance matrices of the measurements and the a priori combined with the Jacobian following Rodgers (2000):

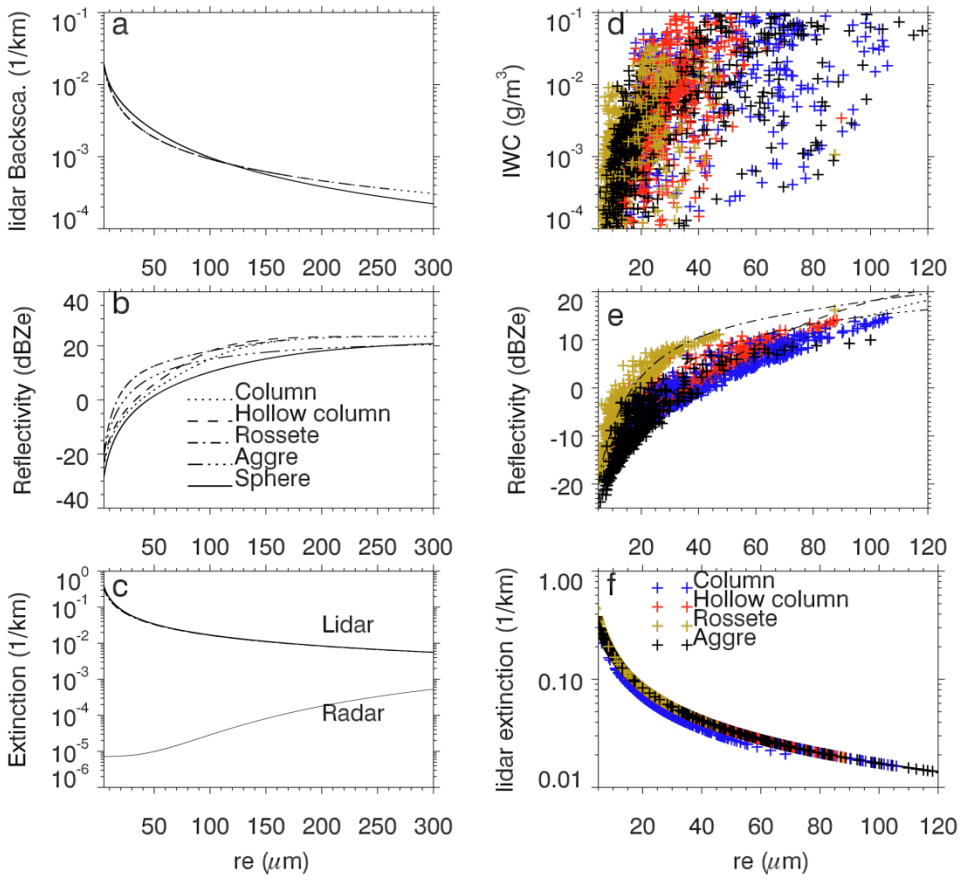

Figure 3. Look-up table comparison assuming Gamma PSD for different habits in a-c. Simulated IWC, IWC normalized extinction and radar reflectivity using in situ PSD are shown in d-f assuming four non-spherical particle habits as in a-c. The symbols denote quantities calculated

from particle spectra measured in situ assuming different particle habits. See the text for more details.

$$S = (K^T S_\varepsilon^{-1} K + S_a^{-1})^{-1} \quad (13)$$

S_ε represents the total measurement error which includes forward model error, random measurement error, and systematic error. If the parameters used in the forward model have large uncertainties, then extra sources of error associated with these parameters must be considered. In the following, we discuss each term for CPR and CALIPSO lidar measurements, respectively.

The radar forward model as described by Eqs. 6, 9, and 10 is sensitive to the assumptions regarding the PSD functional form and the particle habits. According to the look-up-table calculations discussed in section 2.3, for a set of IWC and r_e, the radar forward model can produce different Z_e (varies by 1-5 dB) for different habits. As we choose a habit mixture, an error of about 2.5 dB in Z_e due to the habit assumption is assigned. The CloudSat CPR is well calibrated and validated with CALIPSO-CloudSat Validation Experiments [Tanelli et al., 2008], therefore, the systematic error is less than 1 dB. The random measurement error is due to the limited sample and background noise can be computed from the number of pulses averaged and the linear signal-to-noise ratio of CPR. This term is small compared to the forward model error.

Z_e is parameterized in the lidar-only region (where the Z_e is less than -30 dB) above the lidar/radar overlapped region. The corresponding Z_e error in the lidar-only region is assigned to be 5 dB. This large error assignment ensures that the parameterized radar reflectivity value has minimal contribution on the actual retrieved ice cloud properties in this portion of the layer although the actual information that the radar reflectivity is lower than the minimum detectable by the CRP is retained.

The CALIPSO Lidar instrument error includes the systematic error due to calibration uncertainties as well as random error. The lidar calibration uncertainty is reported to better than 5% using the molecular signal by the CALIPSO science team (Powell, 2009). The random error is evaluated by Liu et al. [2006] from the noise scale factor, the lidar range distance, and the mean and standard deviation of background signal-power.

For the lidar forward model, the principal sources of uncertainty include the assumptions regarding the microphysics (habit and PSD functional form) as well as the uncertainty due to the multiple scattering and lidar ratio approximations. The lidar extinction coefficients vary little for different habits as a function of r_e since r_e is defined to account for shape sensitivity. So the microphysical assumption error is small. The perturbation caused by the η and lidar ratio is significant, then extra sources of error needed to be included in the measurement error covariance by $S_\varepsilon + K_b^T S_b K_b$, where S_b is the parameter error covariance matrix, and K_b is the sensitivity of the forward model to parameters.

2.5 Convergence analysis and Retrieval Status

Testing for convergence is to stop the iteration when change in the solution varies by a small quantity. In our algorithm, we use an appropriate test (equation 5.33) from Rodgers 2000:

$$d_i^2 = [F(x_{i+1}) - F(x_i)]^T S_{\delta y}^{-1} [F(x_{i+1}) - F(x_i)] << m \quad (14)$$

For this retrieval, we specify the criterion of "much less than" in equation (14) such that

$$d_i^2 = [F(x_{i+1}) - F(x_i)]^T S_{\delta y}^{-1} [F(x_{i+1}) - F(x_i)] < 0.01m \quad (15)$$

After the iteration convergence, we compare the difference between the forward model simulations with the measurements. The commonly used method is to compare the difference between the forward model simulation and the measurement with the expected measurement and forward model errors, e.g:

$$\chi^2[y - F(x_i)] = [y - F(x_i)]^T S_\varepsilon^{-1} [y - F(x_i)] \cong m \quad (16)$$

It might be expected to follow a χ^2 distribution with m degrees of freedom. Marks and Rodgers (1993) noted that a typical value of χ^2 for a "moderately good retrieval" is *m*. The quantity χ^2/m is included as an output field in the 2C-ICE product.

Error covariance matrix *Sx* of the retrieved state vector is given by:

$$S_x = (S_a^{-1} + K^T S_y^{-1} K)^{-1} \quad (17)$$

the diagonal elements of *Sx* are variances of the elements of *x* and give a measured *y* of the uncertainty in the retrieval given the covariance of measurements and a priori.

3 Ice Cloud Identification

2C-ICE product identifies ice cloud if the entire layer is composed of pure ice according to the cloud phase in the 2B-CLDCLASS-LIDAR product. It also includes the ice portion of mixed phase layer by using either temperature threshold ($T < -4\ ^0C$) or cloud water top in the stratiform mixed phase layer if it is available in the LIDAR-AUX product.

4 Algorithm Inputs

4.1 CloudSat 2B-GEOPROF Data

The CloudSat 2B-GEOPROF product is the input for CloudSat radar measurement in 2C-ICE algorithm. The retrieval uses the radar reflectivity, the cloud mask, and the gaseous attenuation values from this product.

4.2 CloudSat 2B-GEOPROF-Lidar Data

Cloud Geometrical Profile from combined CPR and CALIPSO Lidar (Mace et al., 2009) data is produced by combining the 2B-GEOPROF data product (Mace et al, 2007) and collocated CALIPSO lidar data to determine the vertical locations of cloud layers.

4.3 CloudSat 2B-CLDCLASS-Lidar Data

2B-CLDCLASS-Lidar (cloud classification from combined CPR and CALIPSO Lidar measurements, refer to CloudSat Standard Data Products) is to identify cloud phases and eight basic types of clouds, so that downstream retrieval algorithms or assumptions can be applied to the conditions for which they are considered valid. Cloud type and cloud phase in the 2B-CLDCLASS product are used to identify ice clouds layers and to screen problematic profiles.

4.4 CloudSat Lidar-AUX Data

CloudSat Lidar-AUX product is to collocate CALIPSO lidar data at CloudSat track but at CALISPO vertical resolution and identify the lidar cloud mask. The cloud layer boundaries are identified based on CloudSat radar measurement and collocated CALIPSO lidar measurements. 2C-ICE identifies ice clouds using the cloud layer types and cloud layer phases. CALIPSO Lidar backscattering coefficient for 2C-ICE input is also from this product.

4.5 CloudSat ECMWF-AUX Data

The retrieval uses temperature information from the CloudSat ECMWF-AUX product, which takes model output from ECMWF and interpolates the variables to the CloudSat data grid. Temperature information is used to assign a priori values in the ice cloud retrieval and also to guide the combination of the ice and liquid information into composite profiles.

5 Algorithm Summary

The algorithm is implemented in Fortran 90. The following is a pseudocode description of the algorithm implementation:

start 2C-ICE
get orbit of 2B-GEOPROF data (CPR cloud mask, radar reflectivity)
get orbit of 2B-GEOPROF-LIDAR data (CloudLayer, CloudLayerTop, CloudLayerBase)
get orbit of 2B-CLDCLASS-LIDAR data (CloudType, CloudPhase)
get orbit of LIDAR-AUX data (Lidar Mask, Attenuated Backscattering Coefficient)
get orbit of ECMWF-AUX data (Temeprature, Pressure)

for-each 2B-GEOPROF vertical profile
    Identify ice cloud mask
    if ice clouds exists **then**

Estimate ice cloud extinction from lidar backscattering only
Define the lidar/radar zone
Parameterize the radar reflectivity in lidar only zone
Run optimal framework
Determine the state vector and measurement vector
Set up a priori for re and IWC
Assign the uncertainties of measurements and a priori
Repeat
calculate K, Se, S_{sy} matrices
calculate F (forward-model) vector
calculate new state vector
calculate convergence d2

end-repeat if d2< 0.01m
calculate re, IWC, optical depth
calculate $\chi 2$
calculate retrieval uncertainties
calculate output percent uncertainties
load output variables
endif (ice cloud exists)
end-for (loop over profiles)
calculate metadata statistics
end 2C-ICE

6 Data Product Output Format

The 2C-ICE data product is written in an HDF-EOS formatted file. It includes geolocation fields, which includes the longitude, latitude height and time of each profile. They are the same as the 2B-GEOPROF file. The retrieved ice cloud properties along with the retrieval convergence analysis are recorded in data fields. Users are directed to the 2C-ICE Interface Control Document (See Appendix A) for a full description of the data and metadata fields contained in the product. Scale factors used in converting file values into science data values are included in the file as HDF variable attributes. Users are encouraged to read scale factors directly from the file (rather than from written documentation), because the scale factors may change.

7 Product Validations with in Situ Measurement

7.1 Case validation during the TC^4 experiment

The NASA TC^4 (Tropical Composition, Cloud and Climate Coupling) field campaign took place during summer 2007 in the tropical Eastern Pacific (Toon et al., 2010). Data collected during

TC^4 provide two kinds of situations for validation of remote sensing algorithms. On several days, the DC-8 flew along the CloudSat/CALIPSO track during the overpass time allowing for direct comparison of cloud properties derived from CloudSat/CALIPSO data with in situ measurements. This allows us to evaluate the algorithm assumptions such as shape, mass/area and size relationships, Z_e-IWC relations, etc. In addition to this direct comparison with the satellites, coordinated flight patterns between the remote sensing ER2 and the in situ DC-8 and WB57 were conducted. The differences between the ER2 measurements and A-Train measurements, such as vertical and horizontal resolution, and fields of view, can be exploited to test the treatment of these sources of uncertainty in the algorithms applied to the A-Train data. Data collected on July 22, 2007 happen to provide a segment of data collected during the A-Train overpass as well as a portion of the flight when the ER2 and DC8 were flying coordinated patterns. In Figure 4, we plotted the ratio of retrieved properties to 2D-S measured as a function of 2D-S measured for data collected within 5km and 30 minutes (black asterisks) and data collected within 3km and 5 minutes (blue asterisks). It is clear that the data collected within close temporal and spatial collocation have better agreement with the in situ measurement from 2D-S.

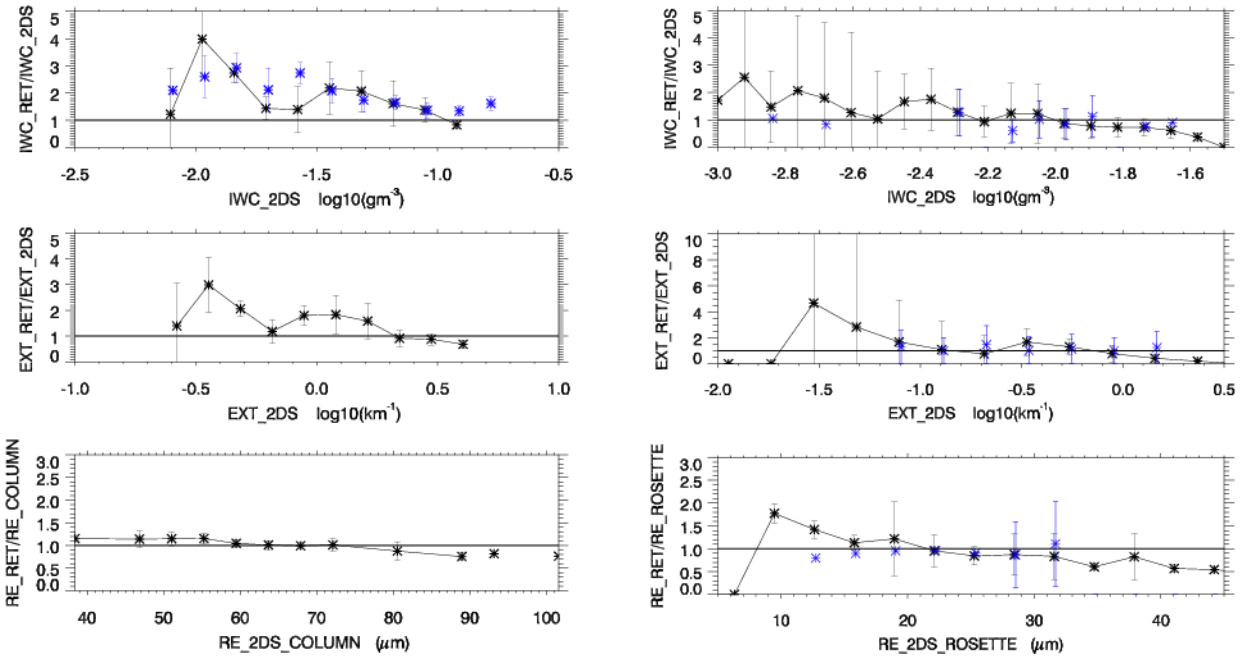

Figure 4 In situ validation of the ER2 case (on the left) and CloudSat/CALIPSO case (on the right) on July 22 with particle size, IWC and extinction measurement on board of DC-8. (a) Ratio of retrieved IWC (black) and CVI measured IWC (blue) with 2D-S measured as a function of 2D-S measured IWC; (b) Ratio of retrieved extinction with 2D-S measured as a function of 2D-S measured extinction; (c) Ratio of retrieved re with 2D-S calculated re assuming habit as

bullet-rosette as a function of 2D-S re. The vertical bars are the standard deviation of the ratios within given bins.

7.2 Case validation during the SPartICus experiment

The recently completed SPartICus (Small Particles in Cirrus) field campaign (Mace et al 2009) was a designed five-month campaign of aircraft measurements in cirrus over the ARM SGP site. It provides a collection of microphysical data, including the 2D stereo probes (2DS), measuring ice particle size distribution $10 < D < 3000$ μm. It is a critical instrument for qualifying concentration of ice cloud particles (Lawson et al 2006). In figure 5, we plotted the minimum distance (*Δdistance*) and time lag (*Δt*) between the SPEC 25 Learjet and A-Train of 17 legs from SPartICus experiments. The sampling temperature ranges from 210 K to 240 K. The distance between the SPEC 25 Learjet and the A-Train satellite tracks ranges from 1-5 km. The time lags between them are within in 15 minutes except for case 3 and 10. Figure 6 shows the case mean ratio and standard deviation of retrieved-to-measured IWC, re and extinction. We can see that standard deviation for IWC and extinction can be as large as factor of 2, while that of re is relative smaller. The deviation could be caused by the location difference, and cloud variation during the sample time duration of two instruments, and the sample errors associated with two instruments. The mean ratios are 1.17, 1.05, and 1.22 for IWC, re, and extinction coefficients, respectively.

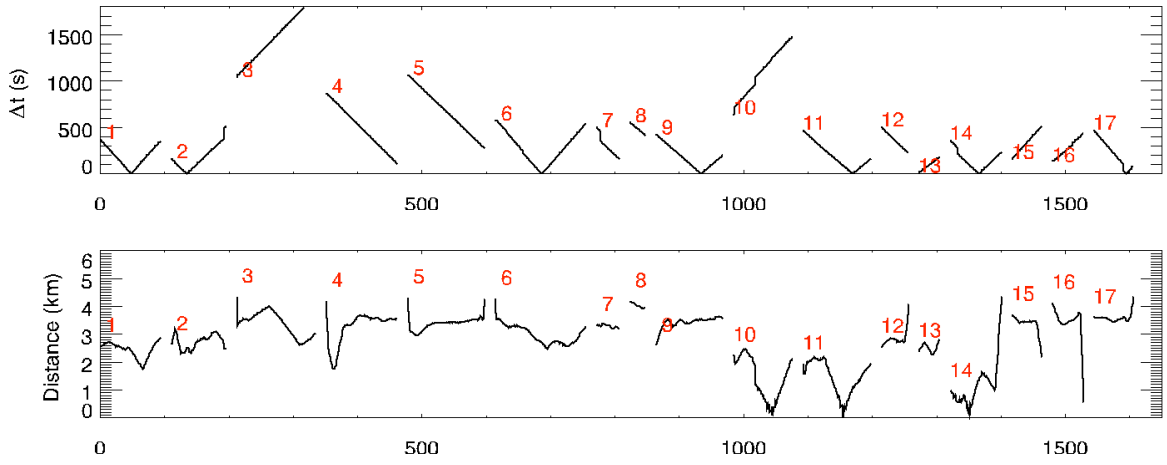

Figure 5. a) Time duration (Δt) between the SPEC LearJet and NASA A-Train for 17 under-flying flights from January to June 2010. b) Minimum distance (Δdistance) between the SPEC Learjet and NASA A-Train.

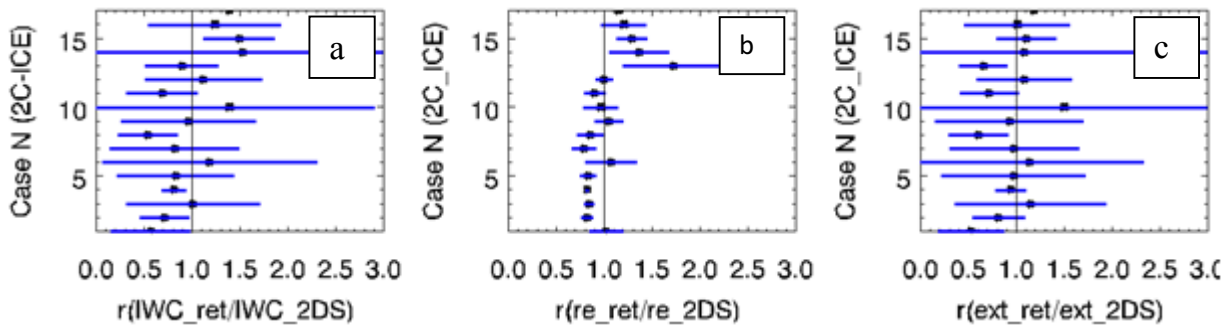

Figure 6. Case mean ratio and standard deviation of retrieved-to-measured IWC, re and extinction coefficients.

8 Changes since version P_R04

In this new version, we improved the Z_e parameterization in the lidar-only region. The relations among Z_e, extinction (σ), and temperature (T) have been more thoroughly investigated using Atmospheric Radiation Measurement (ARM) long-term millimeter cloud radar (MMCR) and Raman lidar measurements (Figure 7).

The new Z_e parameterization is:

$$Ze\ (dBZ) = a + b\times \log 10(\sigma) \times \log 10(T) + c\times \log 10(\sigma) \times T + d\times \log\ 10(\sigma) \qquad (18)$$

where T in K, σ in m^{-1}. The coefficients are listed in Table 1. This Z_e parameterization provides a first order estimation of Z_e as a function extinction and temperature in the lidar-only regions of cirrus layers. The effects of this new parameterization have been evaluated for consistency using radiation closure methods where the radiative fluxes derived from retrieved cirrus profiles compare favorably with CERES measurements (Deng et al 2015).

Table 1 The fitted coefficients of Z_e parameterization as a function of extinction coefficient and temperature: $Z_e(dBZ) = a + b\times \log 10(\sigma) \times \log 10(T) + c\times \log 10(\sigma) \times T + d\times \log 10\ (\sigma)$, where T is in K, σ is in m^{-1}.

Fitting coefficients	**a**	**b**	**c**	**d**
Fitted value	27.2890	6.42015	-0.228607	51.3835

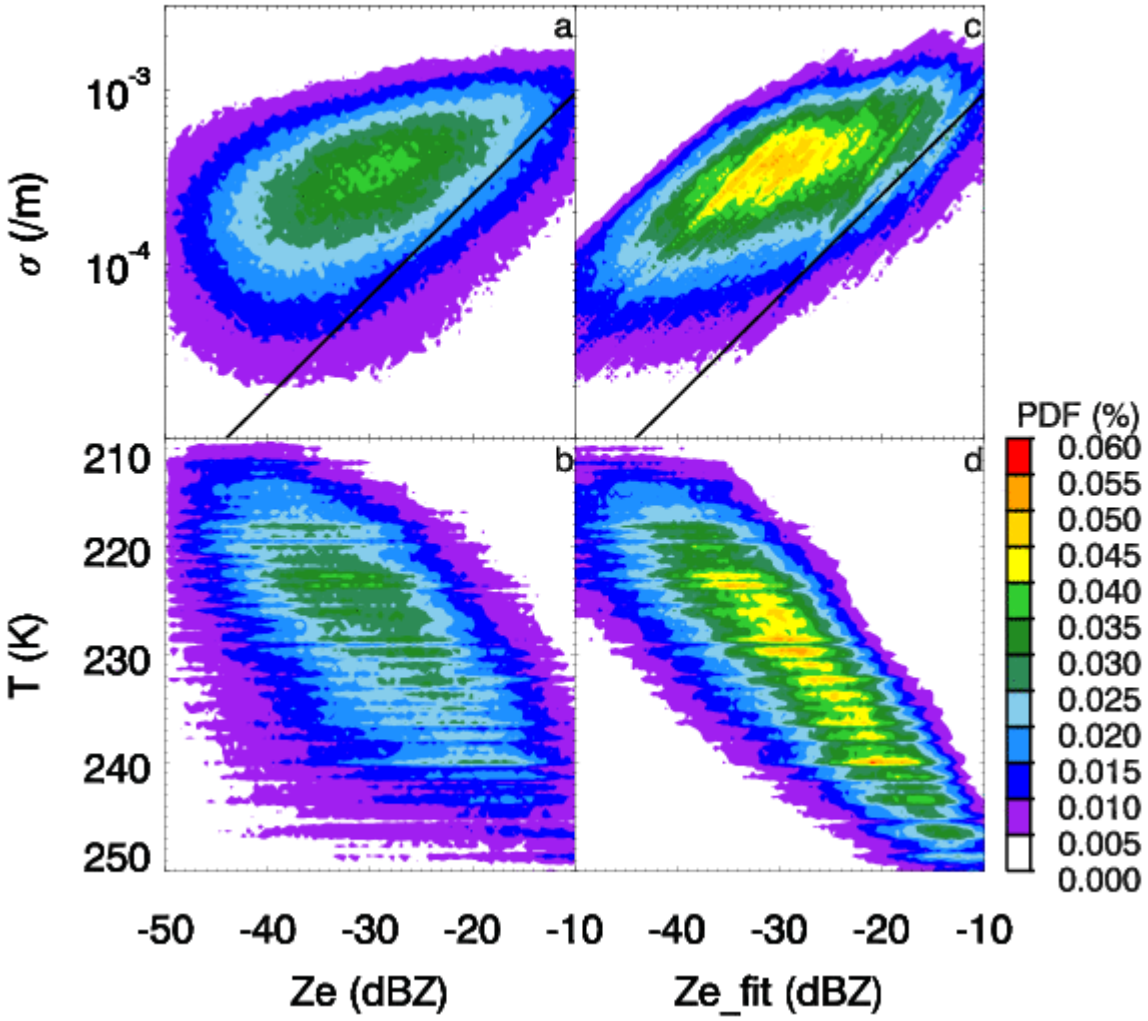

Figure 7 The PDF of Z_e – extinction (σ) and Z_e - T relations from MMCR, Raman lidar and merged sounding data at the ARM SGP site (a and b), and the parameterized Z_e – σ and Z_e-T relations (c and d) from Equ. 18. The black line is derived from the Z_e – σ relation in Matrosov et al. 2003.

9. References

1. Austin, R. T., A. J. Heymsfield, and G. L. Stephens (2009), Retrieval of ice cloud microphysical parameters using the CloudSat millimeter-wave radar and temperature, *J. Geophys. Res.*, 114, D00A23, doi:10.1029/2008JD010049.
2. Battaglia, A., M. O. Ajewole and C. Simmer (2007), Evaluation of radar multiple scattering effects in Cloud-Sat configuration. *Atmos. Chem. Phys.,* in press.
3. Baum B. A. A. J. Heymsfield, P. yang, S. T. Bedka (2005), Bulk scattering properties for the remote sensing of ice clouds. Part I: microphysical data an models. J. Appl, Meteor. 44 1885-1895
4. Brown, P. R. A., and P. N. Francis (1995), Improved measurements of the ice water content in cirrus using a total-water probe. *J. Atmos. Oceanic Technol.,* **12,** 410–414.
5. Deng, M., and G. Mace (2006), Cirrus microphysical properties and air motion statistics using cloud radar Doppler moments. Part I: Algorithm description. *J. Appl. Meteor. Climatol.,* **45,** 1690– 1709.
6. Deng, M., G. G. Mace, Z. Wang, and H. Okamoto (2010), Tropical Composition, Cloud and Climate CouplingExperiment validation for cirrus cloud profiling retrieval using CloudSat radar and CALIPSO lidar, J. Geophys. Res., 115,D00J15, doi:10.1029/2009JD013104
7. Deng, M., Gerald G. Mace, Zhien Wang, and R. Paul Lawson, 2013: Evaluation of Several A-Train Ice Cloud Retrieval Products with In Situ Measurements Collected during the SPARTICUS Campaign. *J. Appl. Meteor. Climatol.*, **52**, 1014–1030.
8. Deng, M., G. G. Mace, Z. Wang, and B. Berry, 2015: CloudSat 2C-ICE product update with a new Ze parameterization in lidar-only region. Submitted to JGR.
9. Delanoe¨, J., and R. J. Hogan (2008), A variational scheme for retrieving ice cloud properties from combined radar, lidar, and infrared radiometer, J. Geophys. Res., 113, D07204, doi:10.1029/2007JD009000
10. Delanoë, J., and R. J. Hogan (2010), Combined CloudSat-CALIPSO-MODIS retrievals of the properties of ice clouds, J. Geophys. Res., 115, D00H29, doi:10.1029/2009JD012346.
11. Eloranta, E. W. (1998), A practical model for the calculation of multiply scattered lidar returns. *Appl. Optics,* **37,** 2464–2472.
12. Fernald R. G. (1983), Analysis of atmospheric lidar observations some comments, Applied Optics. 23. 652-653.
13. Hong G. (2007), Radar backscattering properties of nonspherical ice crystals at 94 GHz. J. Geophy. Res, 112, D22203, doi:10.1029/2007JD008839.
14. Hogan, R. J. (2006), Fast approximate calculation of multiply scattered lidar returns. *Appl. Optics,* **45,** 5984–5992.
15. Lawson, R. P., O'Connor, D., Zmarzly, P., Weaver, K., Baker, B., and Mo, Q.: The 2D-S (Stereo) Probe: Design and Preliminary Tests of a New Airborne, High-Speed, High-Resolution Particle Imaging Probe, J. Atmos. Oceanic Technol., 23, 1462–1477, 2006. 3063
16. Liu, C.-L. and A. J. Illingworth (2000), Towards more accurate retrievals of ice water content from radar measurement of clouds. *J. Appl. Meteorol.,* **39,** 1130–1146.

17. Matrosov, S. Y., M. D. Shupe, A. J. Heymsfield, P. Zuidema (2003), Ice cloud optical thickness and extinction estimates from radar measurements. J. Applied Meterol., 42, 1584-1598.
18. Mace, J.; Jensen, E.; McFarquhar, G.; Comstock, J.; Ackerman, T.; Mitchell, D.; Liu, X.; and Garrett, T., "SPartICus: Small particles in cirrus science and operations plan" (2009). *Publications (E)*. Paper 33.
19. Mace, G. G., R. Marchand, Q. Zhang, and G. Stephens (2007), Global hydrometeor occurrence as observed by CloudSat: Initial observations from summer 2006, *Geophys. Res. Lett.*, *34* (L09808), doi:10.1029/2006GL029017.
20. McFarqhuar, G. M., and A. J. Heymsfield (1997), Parameterization of tropical cirrus ice crystal size distributions and implications for radiative transfer: Results from CEPEX, *J. Atmos. Sci.*,
21. Okamoto, H., S. Iwasaki, M. Yasui, H. Horie, H. Kuroiwa, and H. Kumagai (2003), An algorithm for retrieval of cloud microphysics using 95-GHz cloud radar and lidar. *J. Geophys. Res.,* **108,** 4226–4247.
22. Platt C. and A. C. Dilley (1981), Remote sounding of high clouds. Part III: Monte Carlo calculations of multiple-scattered lidar returns. *J. Atmos. Sci.,* 38, 156-167
23. Powell, K. A., C. A .Hostetler, Z. Liu, M. Vaughan, R. E. Kuehn, W. H. Hunt, K. Lee, C. R. Trepe, R. R. Rogers, S. A. Young (2009), CALIPSO Lidar Calibration Algorithms: Part I –Nighttime 532-nm Parallel Channel and 532-nm Perpendicular Channel *Journal of Atmospheric and Oceanic Technology,* doi: 10.1175/2009JTECHA1242.1
24. Rodgers, C. D. (2000), Inverse Methods for Atmospheric Sounding: Theory and Practice. Series on Atmospheric and Oceanic and Planetary Physics, Vol. 2, World Scientific, 256 .
25. Tanelli, S., S.L. Durden, E. Im, K.S. Pak, D. Reinke, P. Partain, R. Marchand and J. Haynes (2008), "CloudSat's Cloud Profiling Radar after 2 years in orbit: performance, external calibration, and processing", IEEE Transactions on Geoscience and Remote Sensing, November, 2008. Vol.46, Iss.11;.3560-3573
26. Toon, O. B., et al. (2010), Planning, implementation, and first results of the Tropical Composition, Cloud and Climate Coupling Experiment (TC4), J. Geophys. Res., 115, D00J04, doi:10.1029/2009JD013073.
27. Wang, Z. and K. Sassen (2002), Cirrus cloud microphysical property retrieval using lidar and radar measurements - 1. Algorithm description and comparison with in situ data. *J. Appl. Meteorol.,* **41,** 218–229.
28. Yang P. , K. N. Liou, K. Wysler, and D. Mitchell (2000), Parameterization of scattering and absorption properties of individual ice crystals, *J. Geophys. Res*. 105, 4699–4718.
29. Young, Stuart A., Mark A. Vaughan, 2009: The Retrieval of Profiles of Particulate Extinction from Cloud-Aerosol Lidar Infrared Pathfinder Satellite Observations (CALIPSO) Data: Algorithm Description. *J. Atmos. Oceanic Technol.*, **26**, 1105–1119. doi: 10.1175/2008JTECHA1221.1

10. The appendix A: The 2C-ICE Interface Control Document

10.1 I/O Lists

10.1.1 Algorithm Inputs

	Source	Field
(1)	2B-GEOPROF P_R04	Seconds since the start of the granule.
(2)	2B-GEOPROF P_R04	Spacecraft Latitude
(3)	2B-GEOPROF P_R04	Spacecraft Longitude
(4)	2B-GEOPROF P_R04	Height of range bin in Reflectivity/Cloud Mask above reference surface (~ mean sea level).
(5)	2B-GEOPROF P_R04	Data Quality
(6)	2B-GEOPROF P_R04	CPR Cloud Mask
(7)	2B-GEOPROF P_R04	Gaseous_Attenuation
(8)	2B-GEOPROF P_R04	Radar Reflectivity Factor
(9)	2B-GEOPROF P_R04	Digital Elevation Map
(10)	ECMWF-AUX P_R04	Atmospheric pressure
(11)	ECMWF-AUX P_R04	Temperature
(12)	ECMWF-AUX P_R04	Specific humidity
(13)	2B-CLDCLASS-LIDAR P_R04	Cloud Layer
(14)	2B-CLDCLASS-LIDAR P_R04	Cloud Layer Base
(15)	2B-CLDCLASS-LIDAR P_R04	Layer Base Flag
(16)	2B-CLDCLASS-LIDAR P_R04	Cloud Layer Top
(17)	2B-CLDCLASS-LIDAR P_R04	Layer Top Flag
(18)	2B-CLDCLASS-LIDAR P_R04	the logical path of phase determination
(19)	2B-CLDCLASS-LIDAR P_R04	Cloud Phase
(20)	2B-CLDCLASS-LIDAR P_R04	Cloud Phase Confidence Level
(21)	2B-CLDCLASS-LIDAR P_R04	Cloud Layer Type
(22)	2B-CLDCLASS-LIDAR P_R04	Cloud Type Quality
(23)	2B-CLDCLASS-LIDAR P_R04	water layer top
(24)	LIDAR-AUX P_R04	Perpendicular Attenuated Backscatter 532
(25)	LIDAR-AUX P_R04	Total Attenuated Backscatter 532
(26)	LIDAR-AUX P_R04	LidarCloudMask
(27)	LIDAR-AUX P_R04	Day_night_flag
(28)	LIDAR-AUX P_R04	Lidar 60m bin height

10.1.2 Products

10.1.2.1 2C-ICE P_R04 Fields

	Source	Field
(1)	2B-GEOPROF P_R04	Seconds since the start of the granule.
(2)	2B-GEOPROF P_R04	Spacecraft Latitude

	Source	Field
(3)	2B-GEOPROF P_R04	Spacecraft Longitude
(4)	2B-GEOPROF P_R04	Height of range bin in Reflectivity/Cloud Mask above reference surface (~ mean sea level).
(5)	2B-GEOPROF P_R04	UTC seconds since 00:00 Z of the first profile
(6)	2B-GEOPROF P_R04	TAI time for the first profile.
(7)	2B-GEOPROF P_R04	Range to the CPR boresight intercept with the geoid
(8)	2B-GEOPROF P_R04	Digital Elevation Map
(9)	2B-GEOPROF P_R04	Vertical Bin Size
(10)	2B-GEOPROF P_R04	Nominal satellite pitch angle offset from nadir
(11)	2B-GEOPROF P_R04	Nominal satellite roll angle offset from nadir
(12)	ECMWF-AUX P_R04	Temperature
(13)	2B-GEOPROF P_R04	Data Quality
(14)	2B-GEOPROF P_R04	Data status flags
(15)	2B-GEOPROF P_R04	CPR bus orientation (target ID)
(16)	2C-ICE P_R04	apriori effective radius
(17)	2C-ICE P_R04	ice water content a priori
(18)	2C-ICE P_R04	radar signal uncertainty
(19)	2C-ICE P_R04	lidar signal uncertainty
(20)	2C-ICE P_R04	retreived effective radius
(21)	2C-ICE P_R04	retreived IWC
(22)	2C-ICE P_R04	retrieved extinction coefficient
(23)	2C-ICE P_R04	re uncertainty
(24)	2C-ICE P_R04	IWC uncertainty
(25)	2C-ICE P_R04	extinction coefficient uncertainty
(26)	2C-ICE P_R04	retreived IWP
(27)	2C-ICE P_R04	IWP uncertainty
(28)	2C-ICE P_R04	optical depth
(29)	2C-ICE P_R04	optical depth uncertainty
(30)	2C-ICE P_R04	x2/m
(31)	2C-ICE P_R04	nbins of a ice cloudy layer
(32)	2C-ICE P_R04	2C-ICE retrieval status
(33)	2C-ICE P_R04	simulated radar signal from forward model
(34)	2C-ICE P_R04	simulated lidar signal from forward model
(35)	2C-ICE P_R04	radar lidar coverage zone
(36)	2C-ICE P_R04	parameterized radar reflectivity

(37)	2C-ICE P_R04	attenuated backscatter para

10.2 Input Field Specifications

(1) Seconds since the start of the granule.

Name in file: Profile_time
Range: 0 to 6000
Source: 2B-GEOPROF P_R04
Field type (in file): REAL(4)
Field type (in algorithm): REAL(4)
Dimensions: nray
Units: seconds
Missing value:
Missing value operator:
Factor: 1
Offset: 0
MB: 0.139

Seconds since the start of the granule for each profile. The first profile is 0.

(2) Spacecraft Latitude

Name in file: Latitude
Source: 2B-GEOPROF P_R04
Field type (in file): REAL(4)
Field type (in algorithm): REAL(4)
Dimensions: nray
Units: degrees

Spacecraft Geodetic Latitude.

Range: -90 to 90
Missing value:
Missing value operator:
Factor: 1
Offset: 0
MB: 0.139

(3) Spacecraft Longitude

Name in file: Longitude
Source: 2B-GEOPROF P_R04
Field type (in file): REAL(4)
Field type (in algorithm): REAL(4)
Dimensions: nray
Units: degrees

Spacecraft geodetic longitude

Range: -180 to 180
Missing value:
Missing value operator:
Factor: 1
Offset: 0
MB: 0.139

(4) Height of range bin in Reflectivity/Cloud Mask above reference surface (~ mean sea level).

Name in file: Height
Source: 2B-GEOPROF P_R04
Field type (in file): INT(2)
Field type (in algorithm): INT(2)
Dimensions: nbin,nray
Units: m
Range: -5000 to 30000
Missing value: -9999
Missing value operator: ==
Factor: 1
Offset: 0
MB: 8.674

Height of the radar range bins in meters above mean sea level.

(5) Data Quality

Name in file: Data_quality
Source: 2B-GEOPROF P_R04
Field type (in file): UINT(1)
Range: 0 to 127
Missing value:
Missing value operator:
Field type (in algorithm): INT(2)
Dimensions: nray
Units: --
Factor: 1
Offset: 0
MB: 0.035

Flags indicating data quality. If 0, then data is of good quality. Otherwise, treat as a bit field with 8 flags:
0: RayStatus_validity not normal.
1: GPS data not valid.
2: Temperatures not valid.
3: Radar telemetry data quality is not normal. 4: Peak power is not normal.
5: CPR calibration maneuver.
6: Missing frame.
7: Not used.

(6) CPR Cloud Mask

Name in file: CPR_Cloud_mask
Source: 2B-GEOPROF P_R04
Field type (in file): INT(1)
Field type (in algorithm): INT(1)
Dimensions: nbin,nray
Units:
Range: 0 to 40
Missing value: -9
Missing value operator: ==
Factor: 1
Offset: 0
MB: 4.337

Each CPR resolution volume is assigned 1 bit mask value:

0 = No cloud detected
1 = likely bad data
5 = likely ground clutter
5-10 = week detection found using along track integration.
20 to 40 = Cloud detected .. increasing values represents clouds with lower chance of a being a false detection.

(7) Gaseous_Attenuation

Name in file: Gaseous_Attenuation
Source: 2B-GEOPROF P_R04
Field type (in file): INT(2)
Field type (in algorithm): REAL(4)
Dimensions: nbin,nray
Units: dBZe

Gaseous attenuation

Range: 0 to 10
Missing value: -99.99
Missing value operator: ==
Factor: 0.01
Offset: 0
MB: 8.674

(8) Radar Reflectivity Factor

Name in file: Radar_Reflectivity
Source: 2B-GEOPROF P_R04
Range: -40 to 50
Missing value: -88.88
Field type (in file): INT(2)
Field type (in algorithm): REAL(4)

Dimensions: nbin,nray
Units: dBZe
Missing value operator: ==
Factor: 0.01
Offset: 0
MB: 8.674

Radar reflectivity factor Ze is calculated with the echo power and other input data as described in Li and Durden (2001)

(9) Digital Elevation Map

Name in file: DEM_elevation
Source: 2B-GEOPROF P_R04
Field type (in file): INT(2)
Field type (in algorithm): INT(2)
Dimensions: nray
Units: meters
Range: -9999 to 8850
Missing value: 9999
Missing value operator: ==
Factor: 1
Offset: 0
MB: 0.069

Elevation in meters above Mean Sea Level. A value of -9999 indicates ocean. A value of 9999 indicates an error in calculation of the elevation.

(10) Atmospheric pressure

Name in file: Pressure
Source: ECMWF-AUX P_R04
Field type (in file): REAL(4)
Field type (in algorithm): REAL(4)
Dimensions: nbin,nray
Units: Pa

(11) Temperature

Name in file: Temperature
Source: ECMWF-AUX P_R04
Field type (in file): REAL(4)
Field type (in algorithm): REAL(4)
Dimensions: nbin,nray
Units: K

(12) Specific humidity

Name in file: Specific_humidity
Source: ECMWF-AUX P_R04

Field type (in file): REAL(4)
Range: to
Missing value: -999
Missing value operator: ==
Factor: 1
Offset: 0
MB: 17.349
Field type (in algorithm): REAL(4)
Dimensions: nbin,nray
Units: kg/kg

(13)

Name in file: Cloudlayer
Source: 2B-CLDCLASS-LIDAR P_R04
Field type (in file): INT(1)
Field type (in algorithm): INT(1)
Dimensions: nray
Units:
Factor: 1
Offset: 0
MB: 17.349

the total cloud layer by combining radar and lidar measurements

(14)

Name in file: CloudLayerBase
Source: 2B-CLDCLASS-LIDAR P_R04
Field type (in file): REAL(4)
Field type (in algorithm): REAL(4)
Dimensions: ncloud,nray
Units: km
Range: 0 to 1
Missing value: -99
Missing value operator: ==
Factor: 1
Offset: 0
MB: 0.694

Combined cloud base height

(15)

Name in file: LayerBaseFlag
Source: 2B-CLDCLASS-LIDAR P_R04
Field type (in file): INT(1)
Field type (in algorithm): INT(1)
Dimensions: ncloud,nray

Units:
Range: 0 to 20
Missing value: -99
Missing value operator: ==
Factor: 1
Offset: 0
MB: 0.694

For the base 1 for radar and 2 for lidar when both lidar and radar detecte layer. When only lidar detecte a cloud layer, such as supercold water cloud, we assign 3 for it

(16)

Name in file: CloudLayerTop
Source: 2B-CLDCLASS-LIDAR P_R04
Field type (in file): REAL(4)
Field type (in algorithm): REAL(4)
Dimensions: ncloud,nray
Range: 0 to 20
Missing value: -99
Missing value operator: ==
Factor: 1
Offset: 0
Units: km
MB: 0.694

Combined cloud top height

(17)

Name in file: LayerTopFlag
Source: 2B-CLDCLASS-LIDAR P_R04
Field type (in file): INT(1)
Field type (in algorithm): INT(1)
Dimensions: ncloud,nray
Units:
Range: 1 to 3
Missing value: -9
Missing value operator: ==
Factor: 1
Offset: 0
MB: 0.173

For the top 1 for radar and 2 for lidar when both lidar and radar detecte layer. When only lidar detecte a cloud layer, such as supercold water cloud, we assign 3 for it

(18) the logical path of phase determination

Name in file: Phase_log
Source: 2B-CLDCLASS-LIDAR P_R04
Field type (in file): INT(1)

Field type (in algorithm): INT(1)
Dimensions: ncloud,nray
Units:
Range: 0 to 3
Missing value: -9
Missing value operator: ==
Factor: 1
Offset: 0
MB: 0.173

record the logical path of phase determination

(19)

Name in file: CloudPhase
Source: 2B-CLDCLASS-LIDAR P_R04
Field type (in file): INT(1)
Field type (in algorithm): INT(1)
Dimensions: ncloud,nray
Units:
Range: 0 to 2
Missing value: -9
Missing value operator: ==
Factor: 1
Offset: 0
MB: 0.173

Cloud phase identified by using CALIPSO feature, temperature, and radar reflectivity 1-ice, 2-mixed, 3-water

(20)

Name in file: CloudPhaseConfidenceLevel
Source: 2B-CLDCLASS-LIDAR P_R04
Field type (in file): INT(1)
Field type (in algorithm): INT(1)
Dimensions: ncloud,nray
Units:
Range: 0 to 10
Missing value: -9
Missing value operator: ==
Factor: 1
Offset: 0
MB: 0.173

Confidence level assigned to the cloud phase for each layer. It has a value ranging from 0 to 10. 10 indicates the highest confidence level. If confidence level is below 5, use the cloud phase with a caution.

(21)

Name in file: CloudLayerType
Source: 2B-CLDCLASS-LIDAR P_R04
Field type (in file): INT(1)
Field type (in algorithm): INT(1)
Dimensions: ncloud,nray
Units:

Cloud type for each layer. 0 = Not determined
1 = cirrus
2 = Altostratus
3 = Altocumulus 4 = St
5 = Sc
6 = Cumulus
7 = Nimbostratus Cloud 8 = Deep Convection

(22)

Name in file: CloudTypeQuality
Source: 2B-CLDCLASS-LIDAR P_R04
Field type (in file): REAL(4)
Field type (in algorithm): REAL(4)
Dimensions: ncloud,nray
Units:
Range: 0 to 8
Missing value: -9
Missing value operator: ==
Factor: 1
Offset: 0
MB: 0.173

Cloud Type Quality decided based on fuzzy-logic classification.

(23) water layer top

Name in file: Water_layer_top
Source: 2B-CLDCLASS-LIDAR P_R04
Field type (in file): REAL(4)
Field type (in algorithm): REAL(4)
Dimensions: ncloud,nray
Units: km
Range: -9 to 12
Missing value: -9
Missing value operator: ==
Factor: 1
Offset: 0
MB: 0.694

This provides water layer top height in mixed-phase and water clouds. This is mainly to indicate the location of possible water layer in mixed-phase clouds.

(24) Perpendicular Attenuated Backscatter 532

Name in file: PAB532
Source: LIDAR-AUX P_R04
Field type (in file): REAL(4)
Field type (in algorithm): REAL(4)
Dimensions: lidar_l1_583,nray **Units:** km^-1 sr^-1
Range: 0 to 0.2
Missing value: -9999
Missing value operator: ==
Factor: 1
Offset: 0
MB: 80.915

Perpendicular Attenuated Backscatter 532 in a CloudSat footprint

(25) Total Attenuated Backscatter 532

Name in file: TAB532
Source: LIDAR-AUX P_R04
Field type (in file): REAL(4)
Field type (in algorithm): REAL(4)
Dimensions: lidar_l1_583,nray **Units:** km^-1 sr^-1
Range: 0 to 0.4
Missing value: -9999
Missing value operator: ==
Factor: 1
Offset: 0
MB: 80.915

Total Attenuated Backscatter 532 in a CloudSat footprint

(26) LidarCloudMask

Name in file: Mask
Source: LIDAR-AUX P_R04
Field type (in file): INT(1)
Field type (in algorithm): INT(1)
Dimensions: Lidar60m,nray
Units:
Range: 0 to 1
Missing value: -99
Missing value operator: ==
Factor: 1
Offset: 0
MB: 11.936

lidar cloud mask detected at cloudSat footprint and 60 m vertical resolution

(27) Day_night_flag

Name in file: Day_night_flag
Source: LIDAR-AUX P_R04
Field type (in file): INT(1)
Field type (in algorithm): INT(1)
Dimensions: nray
Units:
Range: 0 to 1
Missing value:
Missing value operator:
Factor: 1
Offset: 0
MB: 0.035

Day_night_flag from CALIPSO file: 0 day and 1 night

(28) Lidar 60m bin height

Name in file: height_lidar60m
Source: LIDAR-AUX P_R04
Field type (in file): REAL(4)
Range: -2 to 30
Missing value:
Missing value operator:
Field type (in algorithm): REAL(4)
Dimensions: Lidar60m
Units:
Factor: 1
Offset: 0
MB: 0.001

Lidar 60m bin height used for the 60m cloud mask

10.3 Product Field Specifications

10.3.1 2C-ICE P_R04 Fields

(1) Seconds since the start of the granule.

Name in file: Profile_time
Source: 2B-GEOPROF P_R04
Field type (in file): REAL(4)
Field type (in algorithm): REAL(4)
Dimensions: nray
Units: seconds
Range: 0 to 6000
Missing value:
Missing value operator:
Factor: 1
Offset: 0
MB: 0.139

Seconds since the start of the granule for each profile. The first profile is 0.

(2) Spacecraft Latitude

Name in file: Latitude
Source: 2B-GEOPROF P_R04
Field type (in file): REAL(4)
Field type (in algorithm): REAL(4)
Dimensions: nray
Units: degrees
Spacecraft Geodetic Latitude.
Range: -90 to 90
Missing value:
Missing value operator:
Factor: 1
Offset: 0
MB: 0.139

(3) Spacecraft Longitude

Name in file: Longitude
Source: 2B-GEOPROF P_R04
Field type (in file): REAL(4)
Field type (in algorithm): REAL(4)
Dimensions: nray
Units: degrees
Spacecraft geodetic longitude
Range: -180 to 180
Missing value:
Missing value operator:
Factor: 1
Offset: 0
MB: 0.139

(4) Height of range bin in Reflectivity/Cloud Mask above reference surface (~ mean sea level).

Name in file: Height
Source: 2B-GEOPROF P_R04
Field type (in file): INT(2)
Field type (in algorithm): INT(2)
Dimensions: nbin,nray
Units: m
Range: -5000 to 30000
Missing value: -9999
Missing value operator: ==
Factor: 1
Offset: 0
MB: 8.674

Height of the radar range bins in meters above mean sea level.

(5) UTC seconds since 00:00 Z of the first profile

Name in file: UTC_start
Source: 2B-GEOPROF P_R04
Field type (in file): REAL(4)
Field type (in algorithm): REAL(4)
Dimensions: <scalar>
Units: seconds
Range: 0 to 86400
Missing value:
Missing value operator:
Factor: 1
Offset: 0
MB: 0

The UTC seconds since 00:00 Z of the first profile in the data file.

(6) TAI time for the first profile.

Name in file: TAI_start
Source: 2B-GEOPROF P_R04
Field type (in file): REAL(8)
Field type (in algorithm): REAL(8)
Dimensions: <scalar>
Units: seconds
Range: 0 to 6e+008
Missing value:
Missing value operator:
Factor: 1
Offset: 0
MB: 0

The TAI timestamp for the first profile in the data file. TAI is International Atomic Time: seconds since 00:00:00 Jan 1 1993.

(7) Range to the CPR boresight intercept with the geoid

Name in file: Range_to_intercept
Source: 2B-GEOPROF P_R04
Field type (in file): REAL(4)
Field type (in algorithm): REAL(4)
Dimensions: nray
Units: km
Range: 600 to 800
Missing value:
Missing value operator:
Factor: 1
Offset: 0
MB: 0.139

Range from the spacecraft to the CPR boresight intercept with the geoid.

(8) Digital Elevation Map

Name in file: DEM_elevation **Range:** -9999 to 8850

Source: 2B-GEOPROF P_R04
Missing value: 9999
Field type (in file): INT(2)
Field type (in algorithm): INT(2)
Dimensions: nray
Units: meters
Missing value operator: ==
Factor: 1
Offset: 0
MB: 0.069

Elevation in meters above Mean Sea Level. A value of -9999 indicates ocean. A value of 9999 indicates an error in calculation of the elevation.

(9)

Name in file: Vertical_binsize
Source: 2B-GEOPROF P_R04
Field type (in file): REAL(4)
Field type (in algorithm): REAL(4)
Dimensions: <scalar>
Units: m
Range: to
Missing value: -9999
Missing value operator: ==
Factor: 1
Offset: 0
MB: 0

effective vertical height of the radar range bin.

(10) Nominal satellite pitch angle offset from nadir

Name in file: Pitch_offset
Source: 2B-GEOPROF P_R04
Field type (in file): REAL(4)
Field type (in algorithm): REAL(4)
Dimensions: <scalar>
Units: degrees
Range: -90 to 90
Missing value:
Missing value operator:
Factor: 1
Offset: 0
MB: 0

The pitch angle offset from nadir during normal operations. Pitch up is positive (radar points along the flight track in the direction of motion), down is negative (radar points along the flight track opposite the direction of motion).

(11) Nominal satellite roll angle offset from nadir

Name in file: Roll_offset
Source: 2B-GEOPROF P_R04
Field type (in file): REAL(4)
Field type (in algorithm): REAL(4)
Dimensions: <scalar>
Units: degrees
Range: -90 to 90
Missing value:
Missing value operator:
Factor: 1
Offset: 0
MB: 0

The roll angle offset from nadir during normal operations. Positive roll results in the radar pointing to the right of the flight track. Negative roll to the left.

(12) Temperature

Name in file: Temperature **Range:** to
Source: ECMWF-AUX P_R04
Field type (in file): REAL(4)
Field type (in algorithm): REAL(4)
Dimensions: nbin,nray
Units: K
Missing value: -999
Missing value operator: ==
Factor: 1
Offset: 0
MB: 17.349

(13) Data Quality

Name in file: Data_quality
Source: 2B-GEOPROF P_R04
Field type (in file): UINT(1)
Field type (in algorithm): INT(2)
Dimensions: nray
Units: -- **Range:** 0 to 127
Missing value:
Missing value operator:
Factor: 1
Offset: 0
MB: 0.035

Flags indicating data quality. If 0, then data is of good quality. Otherwise, treat as a bit field with 8 flags:
0: RayStatus_validity not normal.
1: GPS data not valid.
2: Temperatures not valid.
3: Radar telemetry data quality is not normal. 4: Peak power is not normal.
5: CPR calibration maneuver.
6: Missing frame.
7: Not used.

(14) Data status flags

Name in file: Data_status
Source: 2B-GEOPROF P_R04
Field type (in file): UINT(1)
Field type (in algorithm): UINT(1)
Dimensions: nray
Units: --
Range: 0 to 127
Missing value:
Missing value operator:
Factor: 1
Offset: 0
MB: 0.035

This is a bit field that contains data status flags:
Bit 0: missing frame (0=false, 1=true)
Bit 1: SOH missing (0=false, 1=true)
Bit 2: GPS data valid (0=false, 1=true) Bit 3: 1 PPS lost (0=false, 1=true)
Bit 4: Star tracker 1 (0=off, 1=on)
Bit 5: Star tracker 2 (0=off, 1=on)
Bit 6: Coast (0=false, 1=true) Bit 7: NISC (0=false, 1=true)

(15) CPR bus orientation (target ID)

Name in file: Data_targetID
Source: 2B-GEOPROF P_R04
Field type (in file): UINT(1)
Field type (in algorithm): INT(1)
Dimensions: nray
Units: --
Range: 0 to 81
Missing value:
Missing value operator:
Factor: 1
Offset: 0
MB: 0.035

The target id indicates the orientation of the spacecraft bus. For normal operations the target ID is 0. The complete ID table is listed below:

Control Frame 0

0: CPR to point in 300 seconds - Nominal science mode
1 - 15: Target ID for testing - not planned for operational use
Control Frame 0, CPR Calibration
16: CPR to point in 160 seconds
17: CPR 15o to the right
18: CPR 15o to the left
19: CPR 10o to the right -- default rotation
20: CPR 10o to the left -- default rotation
21: CPR 5o to the right
22: CPR 5o to the left
23 - 29: Target ID for testing - not planned for operational use 30 - 36: CPR rotation - not planned for operational use
37 - 39: Not planned for operational use

Control Frame 1, Four thruster closed-loop
40: Rotation into the OR orientation
41: Rotation into the x-track along the anti-ang momentum 42: Rotation into the x-track along ang momentum
43: Rotation into the orbit lower orientation
44: Rotation into alt. OR w/ CPR away from Sun
45 - 49: Not planned for operational use

Control Frame 2, One thruster open-loop
50: Rotation into the OR orientation
51: Rotation into the x-track along the anti-ang momentum 52: Rotation into the x-track along ang momentum
53: Rotation into the orbit lower orientation
54: Rotation into alt. OR w/ CPR away from Sun
55 - 59: Not planned for operational use

Control Frame 3, Two thruster open-loop
60: Rotation into the OR orientation
61: Rotation into the x-track along the anti-ang momentum 62: Rotation into the x-track along ang momentum
63: Rotation into the orbit lower orientation
64: Rotation into alt. OR w/ CPR away from Sun
65 - 69: Not planned for operational use

Control Frame 4, Four thruster open-loop 70: Rotation into the OR orientation
71: Rotation into the x-track along the anti-ang momentum 72: Rotation into the x-track along ang momentum
73: Rotation into the orbit lower orientation
74: Rotation into alt. OR w/ CPR away from Sun

75 - 80: Not planned for operational use

Control Frame 5
81: Body into the x-track along the anti-ang momentum 82 - 1023: Not planned for operational use

(16) apriori effective radius

Name in file: AP_re
Source: 2C-ICE P_R04
Field type (in file): REAL(4)
Field type (in algorithm): REAL(4)
Dimensions: nbin,nray
Units: um
Range: 0 to 500
Missing value: -7777
Missing value operator: <=
Factor: 1
Offset: 0
MB: 17.349

(17) ice water content a priori

Name in file: AP_IWC
Source: 2C-ICE P_R04
Field type (in file): REAL(4)
Field type (in algorithm): REAL(4)
Dimensions: nbin,nray
Units: g/m^3
Range: 0 to 1000
Missing value: -7777
Missing value operator: <=
Factor: 1
Offset: 0
MB: 17.349

(18) radar signal uncertainty

Name in file: dBZe_uncertainty
Source: 2C-ICE P_R04
Field type (in file): REAL(4)
Field type (in algorithm): REAL(4)
Dimensions: nbin,nray
Units:
Range: 0 to 100
Missing value: -7777
Missing value operator:
Factor: 1
Offset: 0
MB: 17.349

(19) lidar signal uncertainty

Name in file: TAB_uncertainty
Source: 2C-ICE P_R04
Field type (in file): REAL(4)
Field type (in algorithm): REAL(4)
Dimensions: nbin,nray
Units:
Range: to
Missing value:
Missing value operator:
Factor: 1
Offset: 0
MB: 17.349

(20) retreived effective radius

Name in file: re
Source: 2C-ICE P_R04
Field type (in file): REAL(4)
Field type (in algorithm): REAL(4)
Dimensions: nbin,nray
Range: 0 to 1000
Units: um
Missing value: -7777
Missing value operator: <=
Factor: 1
Offset: 0
MB: 17.349

(21) retreived IWC

Name in file: IWC
Source: 2C-ICE P_R04
Field type (in file): REAL(4)
Field type (in algorithm): REAL(4)
Dimensions: nbin,nray
Units: g/m^3
Range: to
Missing value:
Missing value operator:
Factor: 1
Offset: 0
MB: 17.349

(22) retrieved extinction coefficient

Name in file: EXT_coef
Source: 2C-ICE P_R04
Field type (in file): REAL(4)
Field type (in algorithm): REAL(4)

Dimensions: nbin,nray
Range: to
Missing value: -7777
Missing value operator:
Factor: 1
Offset: 0
MB: 17.349
Units: /m

(23) re uncertainty

Name in file: re_uncertainty
Source: 2C-ICE P_R04
Field type (in file): REAL(4)
Range: 0 to 250
Missing value: -7777
Missing value operator: <=
Field type (in algorithm): REAL(4)
Dimensions: nbin,nray
Units: %
Factor: 1
Offset: 0
MB: 17.349

(24) IWC uncertainty

Name in file: IWC_uncertainty
Source: 2C-ICE P_R04
Field type (in file): REAL(4)
Field type (in algorithm): REAL(4)
Dimensions: nbin,nray
Units: % **Range:** 0 to 250
Missing value: -7777
Missing value operator: <=
Factor: 1
Offset: 0
MB: 17.349

(25) extinction coefficient uncertainty

Name in file: EXT_coef_uncertainty
Source: 2C-ICE P_R04
Field type (in file): UINT(1)
Field type (in algorithm): REAL(4)
Dimensions: nbin,nray
Units: %
Range: 0 to 250
Missing value: -7777
Missing value operator: <=
Factor: 1
Offset: 0

MB: 4.337

(26) retreived IWP

Name in file: ice_water_path
Source: 2C-ICE P_R04
Field type (in file): REAL(4)
Field type (in algorithm): REAL(4)
Dimensions: nray
Units: g/m^2
Range: to
Missing value: -7777
Missing value operator: <=
Factor: 1
Offset: 0
MB: 0.139

(27) IWP uncertainty

Name in file: ice_water_path_uncertainty
Source: 2C-ICE P_R04
Field type (in file): UINT(1)
Field type (in algorithm): REAL(4)
Dimensions: nray
Units: % **Range:** to
Missing value: -7777
Missing value operator: <=
Factor: 1
Offset: 0
MB: 0.035

(28) optical depth

Name in file: optical_depth
Source: 2C-ICE P_R04
Field type (in file): REAL(4)
Field type (in algorithm): REAL(4)
Dimensions: nray
Units:
Range: to
Missing value: -7777
Missing value operator: <=
Factor: 1
Offset: 0
MB: 0.139

(29) optical depth uncertainty

Name in file: optical_depth_uncertainty
Source: 2C-ICE P_R04
Field type (in file): UINT(1)
Field type (in algorithm): REAL(4)
Dimensions: nray
Units:

(30) x2/m

Name in file: chi_square
Source: 2C-ICE P_R04
Field type (in file): REAL(4)
Field type (in algorithm): REAL(4)
Dimensions: nray
Units:
Range: to
Missing value: -7777
Missing value operator: <=
Factor: 1
Offset: 0
MB: 0.035

(31) nbins of a ice cloudy layer

Name in file: profile_dimension
Source: 2C-ICE P_R04
Field type (in file): INT(1)
Field type (in algorithm): INT(2)
Dimensions: nray
Units:
Range: 0 to 500
Missing value: -7777
Missing value operator: <=
Factor: 1
Offset: 0
MB: 0.035

(32) 2C-ICE retrieval status

Range: to
Missing value: -7777
Missing value operator: <=
Factor: 1
Offset: 0
MB: 0.139
Name in file: cc_ice_status
Source: 2C-ICE P_R04
Field type (in file): INT(2)
Field type (in algorithm): INT(2)
Dimensions: nray
Units:
Range: to
Missing value:

Missing value operator:
Factor: 1
Offset: 0
MB: 0.069

(33) simulated radar signal from forward model

Name in file: dBZe_simulation
Source: 2C-ICE P_R04
Field type (in file): REAL(4)
Field type (in algorithm): REAL(4)
Dimensions: nbin,nray
Units: dbz
Range: to
Missing value: -7777
Missing value operator:
Factor: 1
Offset: 0
MB: 17.349

(34) simulated lidar signal from forward model

Name in file: TAB_simulation
Source: 2C-ICE P_R04
Field type (in file): REAL(4)
Field type (in algorithm): REAL(4)
Dimensions: nbin,nray
Units: /km
Range: to
Missing value:
Missing value operator:
Factor: 1
Offset: 0
MB: 17.349

(35) radar lidar coverage zone

Name in file: zone
Source: 2C-ICE P_R04
Field type (in file): INT(4)
Field type (in algorithm): INT(4)
Dimensions: nbin,nray
Units:
Range: 0 to 255
Missing value: -7777
Missing value operator:
Factor: 1
Offset: 0
MB: 17.349

(36) parameterized radar reflectivity

Name in file: ze_makeup
Source: 2C-ICE P_R04
Field type (in file): REAL(4)
Range: -100 to 100
Missing value: -7777
Missing value operator:
Field type (in algorithm): REAL(4)
Dimensions: nbin,nray
Units: dbz
Factor: 1
Offset: 0
MB: 17.349

(37) attenuated backscatter para

Name in file: tab_para
Source: 2C-ICE P_R04
Field type (in file): REAL(4)
Field type (in algorithm): REAL(4)
Dimensions: nbin,nray
Units: 1/km
Range: to
Missing value:
Missing value operator:
Factor: 1
Offset: 0
MB: 17.349